

Rotation-mediated bosonic Josephson junctions in position and momentum spaces

Sunayana Dutta^{1,2,*} and Ofir E. Alon^{1,2}

¹*Department of Physics, University of Haifa, Haifa 3498838, Israel*

²*Haifa Research Center for Theoretical Physics and Astrophysics,
University of Haifa, Haifa 3498838, Israel*

(Dated: March 14, 2025)

arXiv:2503.10153v1 [cond-mat.quant-gas] 13 Mar 2025

Abstract

In ultracold atoms, bosons tunneling in a double-well potential can produce a typical Josephson junction in real space. A major advancement in quantum matter and simulations is anticipated by the recently found momentum-space Josephson junction effect, which elucidates the supercurrent flow between spin-orbit coupled Bose-Einstein condensates at two distinct independent momentum states. For the first time, our study unveils specific protocols to engineer momentum-space Josephson dynamics for scalar bosons (or a single-component condensate) in a rotating frame through modulation of the geometry of a double-well trapping potential and rotation frequencies. In this setup, rotation simultaneously results in effective double wells both in position and in momentum spaces, and the dynamics of the corresponding Josephson junctions is hosted in these double wells. Consequently, it is observed that the rotation generates momentum-space Josephson dynamics of the condensate along the transverse direction and position-space Josephson dynamics along the longitudinal direction; these effects are particularly noticeable for high rotation frequencies. Additionally, the rotation-induced momentum-space effects are highly significant in both the mean-field and many-body dynamics. Our protocols offer a framework for investigating momentum-space Josephson effects for single-component condensate in both theoretical and experimental contexts, as well as their significant applications in quantum mechanical devices.

Introduction. The Josephson effect [1, 2] is a fascinating quantum phenomenon in which supercurrents flow through two reservoirs coupled by a weak link known as a Josephson junction. On numerous platforms, the Josephson junction has been experimentally realized, extending from solid-state superconductors [3], superfluid Helium [4–8], exciton polaritons [9] to ultracold atoms [10–22]. The latter case, for bosons tunneling in a double-well potential, is commonly referred to as a bosonic Josephson junction (BJJ). Josephson junctions play a crucial role in the development of superconducting quantum interference devices (SQUIDs) [23, 24], superconducting qubits [25–28], and precision measurements [23], due to quantum tunneling of particles across the junction. Exploration of BJJ leads to uncover various intriguing features, including Josephson-like dynamics of a BEC of rubidium atoms [29], universality of fragmentation dynamics of an asymmetric BJJ [30], impact of both the transversal and longitudinal degrees-of-freedom on Josephson dynamics in the resonant

* sdutta@campus.haifa.ac.il

tunneling scenario [31], among others.

In recent times, utilising momentum states as a synthetic degree of freedom for quantum matter and quantum simulations [32] has become more feasible with the realization of the momentum-space Josephson effect. A momentum-space Josephson junction can be realized with a momentum-space double-well dispersion, where the condensates at two distinct band minima can be treated as two distinct independent quantum states. The tunneling of the condensates at these two distinct momenta is not directly coupled. The momentum-space Josephson Junction has been first reported for a spin-orbit coupled BEC located at two discrete momentum states coupled through momentum kicks of laser beams [33]. Beyond the conventional voltage-driven Josephson effect, this work demonstrates how the tunneling phase in the momentum space can generate the Josephson junction. Also, in a Raman-induced spin-orbit-coupled BEC, Ref. [34] experimentally realised the momentum-space Josephson effect, whose double-well band dispersion has two band minima at distinct momentum states that resemble real space Josephson junctions.

In previous work, we have reported the breakup of the ground-state density of rotating bosons in an elongated barrierless trap, for finite systems [35] as well as at the limit of an infinite number of particles [36]. In addition, it is noted that the density fragments into two bosonic clouds in position space along the longitudinal direction and in momentum space in the transverse direction, thereby creating two effective double wells. Hence, the results from this ground-state investigation invoke possible ideas of engineering bosonic Josephson junctions in position and momentum spaces for scalar bosons using rotations. In this Letter, the starting point of our investigation is the impact of rotation on the Josephson dynamics of scalar bosons in a double-well potential. It is intriguing to examine whether rotation can enhance or suppress the Josephson effect in the double-well potential. Further, the possibility of generating the momentum-space Josephson effect is another primordial point. Our work is further extended to unveil a useful protocol, based on the double-well potential, to engineer rotation-induced Josephson effects both in position and momentum spaces for scalar bosons.

Theoretical Method. We consider the multi-configurational time-dependent Hartree method for bosons (MCTDHB) [37, 38] to numerically simulate our system. In MCT-

DHB, the N -boson Hamiltonian can be written as

$$\hat{H} = \sum_{i=1}^N \hat{h}(\mathbf{r}_i) + \sum_{i<j} \hat{W}(|\mathbf{r}_i - \mathbf{r}_j|). \quad (1)$$

Here, $\hat{h}(\mathbf{r}) = \hat{T}(\mathbf{r}) + \hat{V}(\mathbf{r})$ is the one-body operator. In the rotating frame, the kinetic energy in the one-body operator is modified with the angular-momentum operator \hat{l}_z as $\hat{T}(\mathbf{r}) = \frac{1}{2}(\hat{p}_x^2 + \hat{p}_y^2) - \Omega \hat{l}_z$, with Ω being the rotation frequency. In addition, $\hat{V}(\mathbf{r})$ represents the trapping potential. Finally, the two-body operator $\hat{W}(|\mathbf{r} - \mathbf{r}'|) = \frac{\lambda_0}{2\pi\sigma^2} e^{-\frac{(\mathbf{r}-\mathbf{r}')^2}{2\sigma^2}}$ is the repulsive interaction between the bosons. The interaction is modeled by a Gaussian potential as the delta potential does not scatter in two dimensions [39]. $\sigma = 0.25$ is the interaction width, λ_0 is the interaction strength and is scaled with the number of bosons N as $\Lambda = \lambda_0(N - 1)$, where Λ is called the interaction parameter. The MCTDHB method is elaborated in the supplemental material. For the numerical simulation, MCTDH-X software [40–42], which implements the MCTDHB theory, is used. In this work to explore the many-body effects, $N = 10$ interacting bosons with the interaction parameter $\Lambda = 0.04$ are used. We also analyze the mean-field dynamics with fix Λ . For the investigation of the dynamics under rotation, the bosons are initially prepared in the left well $V_L(x, y) = \frac{1}{2}(x + 2)^2 + \frac{1}{2}y^2$ of a double-well potential. To adequately capture the essence of Josephson dynamics, the concept of survival probability in the left well of a double-well trap is used. The survival probability signifies the degree of tunneling of a significant number of bosons from the right to the left well $P_L(t) = \int_{-\infty}^0 \int_{-\infty}^{+\infty} dx dy \frac{\rho(x, y; t)}{N}$, with $\rho(x, y; t)$ being the density of the bosonic cloud, at the instant of time t , when the left well is macroscopically occupied by bosons. All the results in this paper are presented with a modified time frame. Thus, the propagation time is scaled by time period of the dynamics, corresponds to Rabi oscillations of non-interacting bosons in the double-well potential, t_{Rabi} , here $t_{Rabi} = 132.498$.

Rotating a double-well trap and self-trapping. One area that remains largely unexplored is the Josephson dynamics of rotating bosons in a generic double-well potential. Here, the double-well dynamics is approached as a preparatory problem. We proceed further with our investigation on the basis of the findings of the rotating double-well dynamics. The real-space dynamics of bosons in a rotating double-well reveals that rotation gradually slows down the dynamics with the increase of rotation frequencies. Here, the many-body dynamics is prominently affected even at slow rotations by tracing incomplete tunneling with damped oscillations. This signifies the development of quantum correlations in the

system for finite interaction strengths. Hence, rotation imparts a larger tunneling period of the Josephson dynamics, both in the mean-field and many-body domains in the double-well trap. In addition, a specific critical rotation frequency $\Omega_c = 0.5$ leads to complete elimination of tunneling, signaling the emergence of self-trapping. The rotation creates an effective centrifugal barrier in addition to the double-well barrier, which hinders tunneling, thereby on-setting trapping by localizing the bosons in one of the two wells. All the figures and details of the rotating double-well dynamics are collected in the supplemental material.

Protocol to generate a momentum-space Josephson junction. Thus far, we have observed that the rapid rotation eliminates Josephson tunneling in the double-well potential, which results in trapping. The rotation creates an additional effective barrier that prevents the tunneling of bosons in a double-well potential. Here, we provide a protocol to host the Josephson dynamics in the rotating frame. We also now show how to generate a momentum-space Josephson junction with rotation by altering the trap geometry to reduce the additional barrier. The effect of the centrifugal barrier caused by rotation in the double-well potential

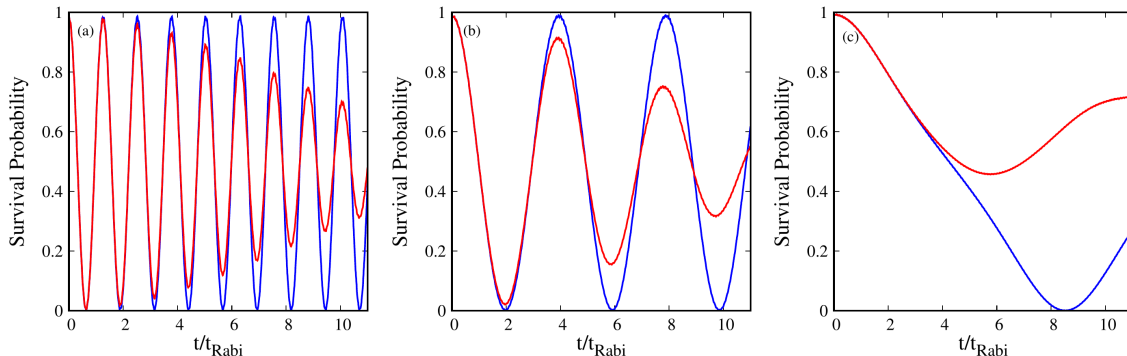


FIG. 1. Dynamics of the survival probability characterizing the position-space Josephson effect are shown for the protocol to generate momentum-space Josephson junction at three various rotation frequencies Ω for interaction strength $\Lambda = 0.04$. Panels (a) corresponds to $\Omega = 0.2$, (b) corresponds to $\Omega = 0.5$, and (c) corresponds to $\Omega = 0.7$. The blue-colored line depicts the mean-field dynamics and the red-colored one represents the many-body dynamics. Beyond the critical rotation frequency of the double-well potential ($\Omega_c = 0.5$), the Josephson effect is prominent for this protocol. All the quantities are dimensionless.

is eliminated in this double-well-based protocol as

$$V_C = V(\mathbf{r}) + \frac{1}{2}\Omega^2(x^2 + y^2). \quad (2)$$

Here, $V(\mathbf{r})$ is the double-well potential used in this work, which is defined by Eq. (5) in the supplemental material. This modification squeezes in the minima of the two potential wells.

At slow rotations ($\Omega = 0.2$), the Josephson dynamics is comparable to that of a non-rotating double well. The mean-field and many-body survival probabilities coincide in short-time dynamics. In long-time dynamics, the mean-field survival probability retains oscillations with constant amplitude, thereby referring to the complete tunneling of the densities; Fig. 1 (a). However, the many-body dynamics shows damped oscillations, which is a signature of the development of quantum correlations in the condensate. At the critical frequency, $\Omega_c = 0.5$, the rotation frequency that kills off the dynamics in a rotating double-well potential, Josephson dynamics is observed with a slightly larger tunneling period, Fig. 1 (b), in contrast to the double-well dynamics. For a notably faster rotation ($\Omega = 0.7$), the Josephson tunneling is still prominent with an enlarged tunneling period; Fig. 1 (c). Here,

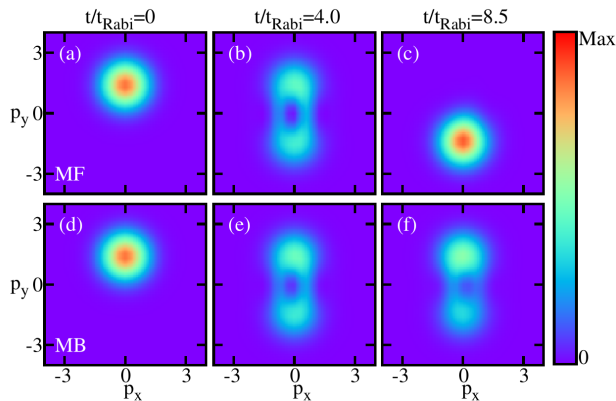


FIG. 2. Time snapshots of the momentum density per particle, which hallmark the emergence of the momentum-space Josephson dynamics for the double-well-based protocol for a specific rotation frequency $\Omega = 0.7$ and interaction strength $\Lambda = 0.04$. Panels (a)-(c) represent the mean-field (MF) momentum densities per particle and (d)-(f) correspond to the many-body (MB) momentum densities per particle. To capture the momentum-space Josephson tunneling, we have opted for three time frames, namely $t_1 = 0$, $t_2 = 4.0$, and $t_3 = 8.5$. All the quantities are dimensionless.

basically, the superposition of the extra-harmonic feed in the double-well potential squeezes the two minima of the combined potential, thereby aiding the Josephson tunneling in this protocol.

The time snapshots of the momentum density profile for fast rotation ($\Omega = 0.7$) are captured in Fig. 2. In order to investigate the dynamics in momentum space, three time

frames, t_1 , t_2 , and t_3 , which represent the three stages of the first tunneling period of the mean-field dynamics in the real space, are used. t_1 refers to the initial time when all bosons are in the left well, and t_2 corresponds to the instant of time when the two wells have identical occupancy. Similarly, t_3 corresponds to the instant of time when all the bosons tunnel towards the right well. The full course of tunneling of the mean-field densities from $+p_y$ to $-p_y$ along the transverse direction of the momentum space, is evident in Fig. 2(a)-(c). However, the tunneling of the many-body densities is much slower than the mean-field counterpart [Fig. 2(d)-(f)], which supplement the incomplete tunneling of the many-body dynamics of the survival probability at $\Omega = 0.7$, see Fig. 1(c). Hence, rotation produces well-localized wavepackets in the momentum space, which renders the onset of Josephson dynamics along the transverse direction p_y in the momentum space. A slight revival of tunneling is also marked in the many-body dynamics [compare Figs.2 (e) & (f)]. For scalar bosons or a single-component BEC, the emergent momentum-space Josephson effect has not been previously documented, as far as we know, in the literature. This protocol not only facilitates Josephson dynamics along the longitudinal direction for strong rotations, but also establishes a Josephson junction in the momentum space along the transverse direction.

Rotation-generated Josephson junctions without a barrier. As an extension, it would be interesting to examine the effects of rotation on the condensate in the case where the double-well barrier is entirely removed. To date, it has not been explored whether rotation will cause any dynamics in a single-well potential.

Fig. 3 depicts the mean-field and many-body dynamics of survival probability in the barrierless trap. In the absence of rotation, the finite interaction of the bosons causes the density to wobble in the single-well potential. As rotation is introduced in the condensate, the tunneling of bosons becomes slightly visible. The Josephson dynamics is prominent at the critical rotation frequency $\Omega_c = 0.5$. However, for fast rotations, $\Omega > \Omega_c$ results in the emergence of trapping.

Several time snapshots of the momentum density profile in the rotating single-well potential are shown in Fig. (4). Interestingly, this study also confirms the presence of a momentum-space Josephson junction along the transverse direction p_y in momentum space. Here, the time frame $t_1 = 0$ is the initial time when all bosons occupied the left well, $t_2 = 2.0$ corresponds to the time when each well is essentially equally populated, and $t_3 = 3.5$ presents the instant of time when all bosons tunnel to the right well. These three time frames corre-

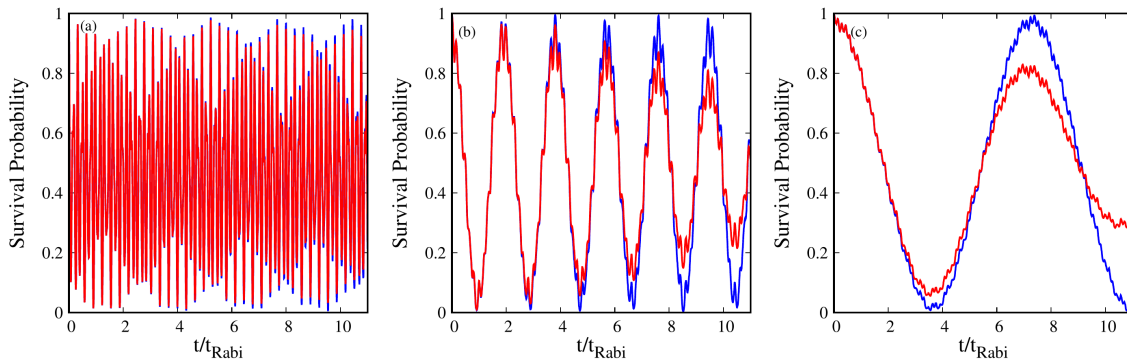


FIG. 3. Dynamics of the survival probability characterizing the Josephson dynamics in position space with various rotation frequencies Ω in a barrierless trap with interaction strength $\Lambda = 0.04$. Panel (a) corresponds to $\Omega = 0$, (b) corresponds to $\Omega = 0.45$, and (c) corresponds to $\Omega = 0.5$. The blue-colored line depicts the mean-field dynamics and the red-colored one represents the many-body dynamics. All the quantities are dimensionless.

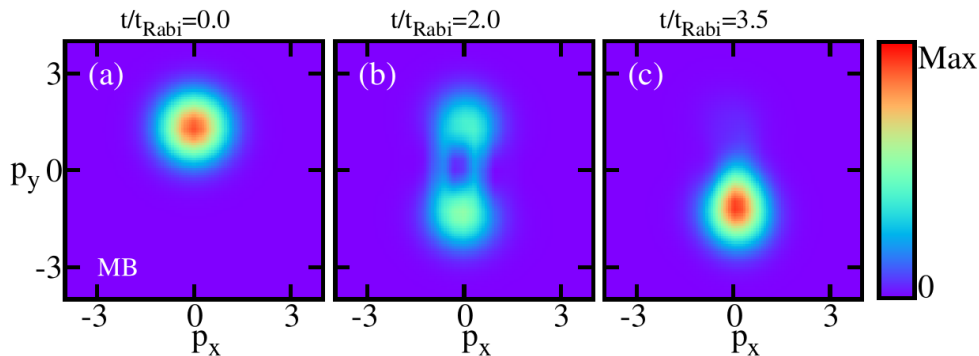


FIG. 4. Time snapshots of the density per particle which hallmark the emergence of the momentum-space Josephson dynamics in a single-well trap for rotation frequency $\Omega = 0.5$ with interaction strength $\Lambda = 0.04$. Panels (a)-(c) represent the many-body (MB) momentum densities per particle. To capture the momentum-space Josephson dynamics, three time frames are chosen, namely $t_1 = 0$, $t_2 = 2.0$, and $t_3 = 3.5$. The significance of these three time frames are elaborated in the main text. All the quantities are dimensionless.

spond to the three stages of the first tunneling period of survival probability. The identical behavior of the mean-field and many-body dynamics of the momentum densities means that the many-body effects are less dominant in the barrierless trap.

In summary, our work has paved the way for engineering Josephson junctions in position

and momentum spaces under rotation by modifying the geometry of a double-well potential. For the first time, rotation is observed to create momentum-space Josephson junctions with scalar bosons, which has so far been achieved only for spin-full bosons with spin-orbit coupling.

Concluding remarks. In a rotating frame, this work offers a method to create a position-space Josephson junction in the longitudinal direction as well as a momentum-space Josephson junction along the transverse direction for scalar or single-component bosons. Here, we report protocols to generate rotation-mediated bosonic Josephson dynamics in both position and momentum spaces by manipulating the geometry of a double-well trap and frequencies of rotation. These momentum-space Josephson junctions are found to have important applications in fabricating novel quantum mechanical devices and in quantum sensors. Due to the higher degree of tunability of the tunneling of the condensate and their stability in a momentum-space Josephson junction, they are very significant for prospective applications in fabricating novel quantum mechanical devices. Our finding may inspire further experimental and theoretical investigation of momentum-space Josephson junction for single-component bosons. Another area of application of our work leads in the direction of exploration of various distinct features of Josephson dynamics by considering momentum state as a synthetic degree of freedom. In the present work, a synthetic gauge field is used to introduce rotation into the condensate. In this context, the rotation can be considered as a particular case of the synthetic gauge field. Thus, the possibility of creating a momentum-space Josephson junction using a synthetic gauge field for scalar bosons would be an intriguing avenue for future research.

ACKNOWLEDGMENTS

This work is supported by the Israel Science Foundation (Grant no. 1516/19). Computation time on the High Performance Computing Center Stuttgart (HLRS) is gratefully acknowledged. S.D. and O.E.A. acknowledge Dr. Axel U. J. Lode for insightful feedback.

-
- [1] B. D. Josephson, Possible new effects in superconductive tunnelling, *Phys. Lett.* **1**, 251 (1962).
 - [2] B. D. Josephson, The discovery of tunnelling supercurrents, *Rev. Mod. Phys.* **46**, 251 (1974).

- [3] P. W. Anderson and J. M. Rowell, Probable observation of the Josephson superconducting tunneling effect, *Phys. Rev. Lett.* **10**, 230 (1963).
- [4] S. Backhaus, S. Pereverzev, A. Loshak, J. Davis, and R. Packard, Direct measurement of the current-phase relation of a superfluid ^3He -b weak link, *Science* **278**, 1435 (1997).
- [5] J. C. Wheatley, Experimental properties of superfluid ^3He , *Rev. Mod. Phys.* **47**, 415 (1975).
- [6] A. J. Leggett, A theoretical description of the new phases of liquid ^3He , *Rev. Mod. Phys.* **47**, 331 (1975).
- [7] K. Sukhatme, Y. Mukharsky, T. Chui, and D. Pearson, Observation of the ideal Josephson effect in superfluid ^4He , *Nature* **411**, 280 (2001).
- [8] E. Hoskinson, R. Packard, and T. M. Haard, Quantum whistling in superfluid helium-4, *Nature* **433**, 376 (2005).
- [9] M. Abbarchi, A. Amo, V. Sala, D. Solnyshkov, H. Flayac, L. Ferrier, I. Sagnes, E. Galopin, A. Lemaître, G. Malpuech, *et al.*, Macroscopic quantum self-trapping and Josephson oscillations of exciton polaritons, *Nature Physics* **9**, 275 (2013).
- [10] F. Dalfovo, L. Pitaevskii, and S. Stringari, Order parameter at the boundary of a trapped Bose gas, *Phys. Rev. A* **54**, 4213 (1996).
- [11] M. Andrews, C. Townsend, H.-J. Miesner, D. Durfee, D. Kurn, and W. Ketterle, Observation of interference between two Bose condensates, *Science* **275**, 637 (1997).
- [12] A. Smerzi, S. Fantoni, S. Giovanazzi, and S. Shenoy, Quantum coherent atomic tunneling between two trapped Bose-Einstein condensates, *Phys. Rev. Lett.* **79**, 4950 (1997).
- [13] P. Öhberg and S. Stenholm, Internal Josephson effect in trapped double condensates, *Phys. Rev. A* **59**, 3890 (1999).
- [14] J. Williams, R. Walser, J. Cooper, E. Cornell, and M. Holland, Nonlinear Josephson-type oscillations of a driven, two-component Bose-Einstein condensate, *Phys. Rev. A* **59**, R31 (1999).
- [15] S. Raghavan, A. Smerzi, S. Fantoni, and S. Shenoy, Coherent oscillations between two weakly coupled Bose-Einstein condensates: Josephson effects, π oscillations, and macroscopic quantum self-trapping, *Phys. Rev. A* **59**, 620 (1999).
- [16] M. Albiez, R. Gati, J. Fölling, S. Hunsmann, M. Cristiani, and M. K. Oberthaler, Direct Observation of Tunneling and Nonlinear Self-Trapping in a Single Bosonic Josephson Junction, *Phys. Rev. Lett.* **95**, 010402 (2005).

- [17] S. Levy, E. Lahoud, I. Shomroni, and J. Steinhauer, The ac and dc Josephson effects in a Bose–Einstein condensate, *Nature* **449**, 579 (2007).
- [18] T. Zibold, E. Nicklas, C. Gross, and M. K. Oberthaler, Classical bifurcation at the transition from Rabi to Josephson dynamics, *Phys. Rev. Lett.* **105**, 204101 (2010).
- [19] G. Spagnolli, G. Semeghini, L. Masi, G. Ferioli, A. Trenkwalder, S. Coop, M. Landini, L. Pezzè, G. Modugno, M. Inguscio, *et al.*, Crossing over from attractive to repulsive interactions in a tunneling bosonic Josephson junction, *Phys. Rev. Lett.* **118**, 230403 (2017).
- [20] A. Burchianti, F. Scazza, A. Amico, G. Valtolina, J. Seman, C. Fort, M. Zaccanti, M. Inguscio, and G. Roati, Connecting dissipation and phase slips in a Josephson junction between fermionic superfluids, *Phys. Rev. Lett.* **120**, 025302 (2018).
- [21] N. Luick, L. Sobirey, M. Bohlen, V. P. Singh, L. Mathey, T. Lompe, and H. Moritz, An ideal Josephson junction in an ultracold two-dimensional Fermi gas, *Science* **369**, 89 (2020).
- [22] G. Valtolina, A. Burchianti, A. Amico, E. Neri, K. Khani, J. A. Seman, A. Trombettoni, A. Smerzi, M. Zaccanti, M. Inguscio, *et al.*, Josephson effect in fermionic superfluids across the BEC-BCS crossover, *Science* **350**, 1505 (2015).
- [23] Y. Makhlin, G. Schön, and A. Shnirman, Quantum-state engineering with Josephson-junction devices, *Rev. Mod. Phys.* **73**, 357 (2001).
- [24] C. Ryu, P. Blackburn, A. Blinova, and M. Boshier, Experimental realization of Josephson junctions for an atom SQUID, *Phys. Rev. Lett.* **111**, 205301 (2013).
- [25] J. M. Martinis, S. Nam, J. Aumentado, and C. Urbina, Rabi oscillations in a large Josephson-junction qubit, *Phys. Rev. Lett.* **89**, 117901 (2002).
- [26] O. Astafiev, Y. A. Pashkin, Y. Nakamura, T. Yamamoto, and J. Tsai, Temperature Square Dependence of the Low Frequency $1/f$ Charge Noise in the Josephson Junction Qubits, *Phys. Rev. Lett.* **96**, 137001 (2006).
- [27] J. M. Martinis, M. Ansmann, and J. Aumentado, Energy Decay in Superconducting Josephson-Junction Qubits from Nonequilibrium Quasiparticle Excitations, *Phys. Rev. Lett.* **103**, 097002 (2009).
- [28] H. Paik, D. I. Schuster, L. S. Bishop, G. Kirchmair, G. Catelani, A. P. Sears, B. Johnson, M. Reagor, L. Frunzio, L. I. Glazman, *et al.*, Observation of High Coherence in Josephson Junction Qubits Measured in a Three-Dimensional Circuit QED Architecture, *Phys. Rev. Lett.* **107**, 240501 (2011).

- [29] J. Vargas, M. Nuske, R. Eichberger, C. Hippler, L. Mathey, and A. Hemmerich, Orbital many-body dynamics of Bosons in the second Bloch band of an optical lattice, *Phys. Rev. Lett.* **126**, 200402 (2021).
- [30] K. Sakmann, A. I. Streltsov, O. E. Alon, and L. S. Cederbaum, Universality of fragmentation in the Schrödinger dynamics of bosonic Josephson junctions, *Phys. Rev. A* **89**, 023602 (2014).
- [31] A. Bhowmik and O. E. Alon, Longitudinal and transversal resonant tunneling of interacting bosons in a two-dimensional Josephson junction, *Sci. Rep.* **12**, 627 (2022).
- [32] F. A. An, E. J. Meier, J. Ang'ong'a, and B. Gadway, Correlated dynamics in a synthetic lattice of momentum states, *Phys. Rev. Lett.* **120**, 040407 (2018).
- [33] J. Hou, X.-W. Luo, K. Sun, T. Bersano, V. Gokhroo, S. Mossman, P. Engels, and C. Zhang, Momentum-space Josephson effects, *Phys. Rev. Lett.* **120**, 120401 (2018).
- [34] A. Mukhopadhyay, X.-W. Luo, C. Schimelfenig, M. Ome, S. Mossman, C. Zhang, and P. Engels, Observation of Momentum Space Josephson Effects in Weakly Coupled Bose-Einstein Condensates, *Phys. Rev. Lett.* **132**, 233403 (2024).
- [35] S. Dutta, A. U. J. Lode, and O. E. Alon, Fragmentation and correlations in a rotating Bose–Einstein condensate undergoing breakup, *Sci. Rep.* **13**, 3343 (2023).
- [36] S. Dutta, A. U. J. Lode, and O. E. Alon, Condensates Breaking Up Under Rotation, *J. Phys.: Conf. Ser.* **2894**, 012014 (2024).
- [37] A. I. Streltsov, O. E. Alon, and L. S. Cederbaum, Role of excited states in the splitting of a trapped interacting Bose-Einstein condensate by a time-dependent barrier, *Phys. Rev. Lett.* **99**, 030402 (2007).
- [38] O. E. Alon, A. I. Streltsov, and L. S. Cederbaum, Multiconfigurational time-dependent Hartree method for bosons: Many-body dynamics of bosonic systems, *Phys. Rev. A* **77**, 033613 (2008).
- [39] R. A. Doganov, S. Klaiman, O. E. Alon, A. I. Streltsov, and L. S. Cederbaum, Two trapped particles interacting by a finite-range two-body potential in two spatial dimensions, *Phys. Rev. A* **87**, 033631 (2013).
- [40] A. U. J. Lode, C. Lévêque, L. B. Madsen, A. I. Streltsov, and O. E. Alon, Colloquium : Multiconfigurational time-dependent Hartree approaches for indistinguishable particles, *Rev. Mod. Phys.* **92**, 011001 (2020).
- [41] A. U. J. Lode, M. Tsatsos, E. Fasshauer, R. Lin, L. Papariello, P. Molognini, C. Lévêque, and S. Weiner, MCTDH-X: The time-dependent multiconfigurational Hartree for indistinguishable

- particles software (2019).
- [42] R. Lin, P. Mognini, L. Papariello, M. C. Tsatsos, C. L ev eque, S. E. Weiner, E. Fasshauer, R. Chitra, and A. U. J. Lode, MCTDH-X: The multiconfigurational time-dependent Hartree method for indistinguishable particles software, *Quantum Sci. Technol.* **5**, 024004 (2020).
 - [43] M. H. Beck, A. J ackle, G. A. Worth, and H. D. Meyer, The multiconfiguration time-dependent Hartree (MCTDH) method: A highly efficient algorithm for propagating wavepackets, *Phys. Rep.* **324**, 1 (2000).
 - [44] H. Wang and M. Thoss, Multilayer formulation of the multiconfiguration time-dependent Hartree theory, *J. Chem. Phys.* **119**, 1289 (2003).
 - [45] U. Manthe, A multilayer multiconfigurational time-dependent Hartree approach for quantum dynamics on general potential energy surfaces, *J. Chem. Phys.* **128**, 164116 (2008).
 - [46] H. Wang, Multilayer Multiconfiguration Time-Dependent Hartree Theory, *J. Phys. Chem. A* **119**, 7951 (2015).
 - [47] U. Manthe and T. Weike, On the multi-layer multi-configurational time-dependent Hartree approach for bosons and fermions, *J. Chem. Phys.* **146**, 064117 (2017).
 - [48] U. Manthe, Wavepacket dynamics and the multi-configurational time-dependent Hartree approach, *J. Phys.: Condens. Matter* **29**, 253001 (2017).
 - [49] A. U. Lode, K. Sakmann, O. E. Alon, L. S. Cederbaum, and A. I. Streltsov, Numerically exact quantum dynamics of bosons with time-dependent interactions of harmonic type, *Phys. Rev. A* **86**, 063606 (2012).
 - [50] P. A. M. Dirac, Note on Exchange Phenomena in the Thomas Atom, *Math. Proc. Cambridge Philos. Soc.* **26**, 376 (1930).
 - [51] N. F. Mott and J. Frenkel, *Math. Gaz.*, Vol. 18 (Clarendon Press, Oxford, 1934) p. 208.
 - [52] P. Kramer and M. Saraceno, *Geometry of the time-dependent variational principle in quantum mechanics* (Springer, Lecture Notes in Physics, 2007).
 - [53] O. Penrose and L. Onsager, Bose-Einstein Condensation and Liquid Helium, *Phys. Rev.* **104**, 576 (1956).
 - [54] R. Spekksens and J. Sipe, Spatial fragmentation of a Bose-Einstein condensate in a double-well potential, *Phys. Rev. A* **59**, 3868 (1999).
 - [55] S. Klaiman and O. E. Alon, Variance as a sensitive probe of correlations, *Phys. Rev. A* **91**, 063613 (2015).

- [56] O. E. Alon, Analysis of a trapped Bose-Einstein condensate in terms of position, momentum, and angular-momentum variance, *Symmetry* **11**, 1344 (2019).
- [57] O. E. Alon, Variance of a Trapped Bose-Einstein Condensate, *J. Phys.: Conf. Ser.* **1206**, 012009 (2019)

SUPPLEMENTAL MATERIAL TO ROTATION-MEDIATED BOSONIC JOSEPHSON JUNCTIONS IN POSITION AND MOMENTUM SPACES

This supplemental material gives further analysis that supports our main results. Sec. S1 provides a detailed theoretical description of the MCTDHB method in the rotating frame. The MCTDHB method is employed in the MCTDH-X software, which is used for the numerical computations of the main results. Sec. S2 provides a more elaborate analysis of the impact of rotation on the dynamics of bosons in a double-well potential. Sec. S3 gives the convergence of the Josephson dynamics with respect to the number of self-consistent orbitals. Here, the convergence checks of the Josephson dynamics are described with the help of survival probability, depletion, and many-particle position and momentum variances, all with respect to the number of self-consistent orbitals. Sec. S4 presents the convergence of the Josephson dynamics with respect to the number of grid points used for the numerical simulations.

S1. MCTDHB IN THE ROTATING FRAME

In this work, a well established many-body numerical method named as the multiconfigurational time-dependent Hartree method for bosons (MCTDHB) [37, 38] is used to accurately solve the Schrödinger equation at the many-body level for ultracold bosons. Here, the MCTDHB approach is the bosonic version of the MCTDH family of methods [43–48] which is able to self-consistently describe the physics involving the presence of many-body correlations. For the numerical simulations, we consider a system of weakly interacting bosons confined in a double-well potential in the rotating frame. The dynamical properties of these trapped bosons can be described by the (time-dependent) many-body Schrödinger equation. The Schrödinger equation that deals with a many-boson system is solved with the help of the mean-field Gross-Pitaevskii approximation. However, the Gross-Pitaevskii approximation is unable to capture many-body features such as fragmentation and correlations, owing to its building via the mean-field ansatz, which has only a single basis state. The MCTDHB method uses the (time-dependent) optimized one-body basis (orbital). The set of bases and the expansion coefficients in the MCTDHB basis are optimized variationally [37, 38]. In addition, the MCTDHB method is in principle numerically exact [49] and able to describe

both coherent and fragmented condensates. One can say the theory of Gross-Pitaevskii approximation is a special case of MCTDHB, when only a single one-body orbital is in use.

A. Many-body Hamiltonian

The Hamiltonian of N interacting bosons is given as

$$\hat{H} = \sum_{j=1}^N \hat{h}(\mathbf{r}_j) + \sum_{j < k} \hat{W}(\mathbf{r}_j - \mathbf{r}_k), \quad (3)$$

with the one-body Hamiltonian

$$\hat{h}(\mathbf{r}) = \hat{T}(\mathbf{r}) + \hat{V}(\mathbf{r}) \quad (4)$$

which is composed of the kinetic energy term $\hat{T}(\mathbf{r})$ and the external potential energy term, which is the trapping potential, $\hat{V}(\mathbf{r})$. In this work, to explore the dynamics, we consider the confining potential to be a double well potential of the form,

$$V(\mathbf{r}) = \begin{cases} \frac{1}{2}(x+2)^2 + \frac{1}{2}y^2; & x < -2, & -\infty < y < \infty \\ \alpha \left(\frac{1}{2}(x+2)^2 + \frac{1}{2}y^2 \right); & -2 \leq x < -\frac{1}{2}, & -\infty < y < \infty \\ \alpha \left(\frac{3}{2}(1-x^2) + \frac{1}{2}y^2 \right); & -\frac{1}{2} \leq x \leq \frac{1}{2}, & -\infty < y < \infty \\ \alpha \left(\frac{1}{2}(x-2)^2 + \frac{1}{2}y^2 \right); & \frac{1}{2} < x < 2, & -\infty < y < \infty \\ \frac{1}{2}(x-2)^2 + \frac{1}{2}y^2; & x > +2, & -\infty < y < \infty \end{cases} \quad (5)$$

Here, α scales the barrier height of $V(\mathbf{r})$ (for double well $\alpha = 1$ and for single well $\alpha = 0$). The two-body interaction of ultracold dilute bosonic gases is considered to be a finite-range interaction and is modeled by a Gaussian function [39], $\hat{W}(\mathbf{r} - \mathbf{r}') = \frac{\lambda_0}{2\pi\sigma^2} e^{-\frac{(\mathbf{r}-\mathbf{r}')^2}{2\sigma^2}}$ with $\sigma = 0.25$. This avoids regularization of the delta contact potential in 2D. The interaction strength λ_0 is scaled with the number of bosons N as $\Lambda = \lambda_0(N - 1)$, where Λ is the interaction parameter. The interaction parameter is used to characterize the mean-field solution. In this work, we use units $\hbar = m = 1$, and all quantities are dimensionless.

The rotation induces modification in the kinetic energy operator as,

$$\hat{T}(\mathbf{r}) = \frac{1}{2}(\hat{p}_x^2 + \hat{p}_y^2) - \Omega \hat{l}_z, \quad (6)$$

here Ω is the rotation frequency and $\hat{l}_z = \hat{x}\hat{p}_y - \hat{y}\hat{p}_x$ is the angular-momentum operator.

Another alternative way to introduce rotation in the condensate is by referring to the concept of rotation as a special case of a synthetic gauge field. Hence, with a gauge field $\mathbf{A}(\mathbf{r})$ the kinetic energy operator in the one-body Hamiltonian is modified as,

$$\hat{T}(\mathbf{r}) = \frac{1}{2}[-i\nabla_{\mathbf{r}} - q\mathbf{A}(\mathbf{r})]^2. \quad (7)$$

The following general gauge field is considered to mimic the effect of rotation:

$$\mathbf{A}(\mathbf{r}) = (ay, bx, 0). \quad (8)$$

Further, expansion of $\hat{T}(\mathbf{r})$ [Equation (7)] gives,

$$\hat{T}(\mathbf{r}) = \frac{1}{2}(\hat{p}_x - ay)^2 + \frac{1}{2}(\hat{p}_y - bx)^2 = \frac{1}{2}(\hat{p}_x^2 + \hat{p}_y^2) - (\hat{p}_x ay + \hat{p}_y bx) + \frac{1}{2}(a^2 y^2 + b^2 x^2). \quad (9)$$

Specifically, if we use $b = -a$, Equation (9) becomes

$$\hat{T}(\mathbf{r}) = \frac{1}{2}(\hat{p}_x^2 + \hat{p}_y^2) - a\hat{l}_z + \frac{1}{2}a^2(y^2 + x^2). \quad (10)$$

We get the following expression of one-body Hamiltonian by combining Equations (4), (6) and (10),

$$\hat{h}(\mathbf{r}) = \hat{T}(\mathbf{r}) + \hat{V}'(\mathbf{r}), \quad (11)$$

where the modified confining potential is $\hat{V}'(\mathbf{r}) = \hat{V}(\mathbf{r}) + \frac{1}{2}a^2\mathbf{r}^2$ and $a = \Omega$ represents the rotation frequency of the condensate.

B. The MCTDHB method

Time-adaptive orbitals are used in the MCTDHB method to represent the field operator as a sum of the M time-dependent single-particle eigenstates,

$$\hat{\Psi}(\mathbf{r}, t) = \sum_{j=1}^M \hat{b}_j \phi_j(\mathbf{r}, t). \quad (12)$$

The MCTDHB ansatz is given as,

$$|\Psi(t)\rangle = \sum_{\vec{n}} C_{\vec{n}} |\vec{n}, t\rangle. \quad (13)$$

In Equation (13), \sum runs over all $\binom{N+M-1}{N}$ possible time-dependent configurations $\vec{n} = (n_1, \dots, n_M)$ with constant particle number $N = \sum_{i=1}^M n_i$. The time-dependent variational

principle [50–52] is employed for the ansatz in Equation (13) to derive the MCTDHB equations. The functional action of the time-dependent Schrödinger equation with the many-body ansatz Equation (13), in the Lagrangian formulation, can be written as [37, 38],

$$S[\{C_{\vec{n}}(t)\}, \{\phi_j(\mathbf{r}, t)\}] = \int dt \{ \langle \Psi | \hat{H} - i \frac{\partial}{\partial t} | \Psi \rangle - \sum_{j,k=1}^M \mu_{jk}(t) [\langle \phi_j | \phi_k \rangle - \delta_{jk}] \}, \quad (14)$$

where the time-dependent Lagrange multipliers $\mu_{jk}(t)$ are introduced to maintain orthonormality of the time-dependent orbitals during propagation. This results in two coupled equations of motion – a set of linear equations for the coefficients $\{C_{\vec{n}}\}$

$$H_{\vec{n}\vec{n}'}(t)C_{\vec{n}}(t) = i \frac{\partial C_{\vec{n}}(t)}{\partial t}, \quad (15)$$

with the matrix $H_{\vec{n}\vec{n}'} = \langle \vec{n}; t | \hat{H} | \vec{n}'; t \rangle$ being time-dependent and a set of non-linear equations for the orbitals $\{\phi_j(\mathbf{r}, t); j = 1, \dots, M\}$,

$$i|\dot{\phi}_j\rangle = \hat{\mathbf{P}} \left[\hat{h}|\phi_j\rangle + \sum_{k,s,q,l=1}^M \{\rho(t)\}_{jk}^{-1} \rho_{ksql} \hat{W}_{sl}|\phi_q\rangle \right]. \quad (16)$$

Here, $\hat{\mathbf{P}} = 1 - \sum_{j'=1}^M |\phi_{j'}\rangle\langle\phi_{j'}|$ is the projection operator, $\rho_{jk} = \langle \Psi | \hat{a}_j^\dagger \hat{a}_k | \Psi \rangle$ and $\rho_{ksql} = \langle \Psi | \hat{a}_k^\dagger \hat{a}_s^\dagger \hat{a}_q \hat{a}_l | \Psi \rangle$ are the matrix elements of the one-body and two-body reduced density matrices (RDM). $\hat{w}_{sl} = \int d\mathbf{r}' \hat{\phi}_s^*(\mathbf{r}'; t) \hat{W}(\mathbf{r} - \mathbf{r}') \hat{\phi}_l(\mathbf{r}; t)$ are the matrix elements of the two-body interaction potential, see Refs. [37, 38] for more details and the derivation of the equations of motion.

C. Quantities of interest

We discuss the quantities of interest, namely the concept of the one-body reduced density matrix, the eigenvalues of the one-body reduced density matrix (RDM), and the many-particle variances of the position and momentum operators here. These quantities would assist us to explore the dynamics of bosons.

1. One-body reduced density matrix (RDM), one-body density, and natural occupations

For the N-boson state $|\Psi\rangle$, the one-body RDM is a hermitian matrix and given as

$$\rho^{(1)}(\mathbf{r}, \mathbf{r}'; t) = \langle \Psi | \hat{\Psi}^\dagger(\mathbf{r}') \hat{\Psi}(\mathbf{r}) | \Psi \rangle = \sum_{k,q} \rho_{kq} \phi_k^*(\mathbf{r}', t) \phi_q(\mathbf{r}, t) \quad (17)$$

with eigenbases $\{\phi_q(\mathbf{r}, t)\}$. $\rho_{kq} = \langle \Psi | \hat{b}_k^\dagger \hat{b}_q | \Psi \rangle$ represent the matrix elements of the one-body RDM with M orbitals corresponding to the creation (annihilation) operators \hat{b}_k^\dagger (\hat{b}_q). The diagonal of $\rho^{(1)}(\mathbf{r}, \mathbf{r}'; t)$ is termed the one-body density $\rho(\mathbf{r}, t)$ and it can be written as $\rho(\mathbf{r}, t) = \rho^{(1)}(\mathbf{r}, \mathbf{r}' = \mathbf{r}; t)$. The eigenvalues of the one-body RDM are achieved by the diagonalization of Equation (17) which corresponds to a unitary transformation of the orbitals $\phi_q(\mathbf{r}, t)$ to the natural orbitals $\phi_j^{(NO)}(\mathbf{r}, t)$ as

$$\frac{\rho^{(1)}(\mathbf{r}, \mathbf{r}'; t)}{N} = \sum_j n_j(t) \phi_j^{(NO),*}(\mathbf{r}', t) \phi_j^{(NO)}(\mathbf{r}, t). \quad (18)$$

The eigenvalues n_j are normalized as $\sum_{j=1}^M n_j(t) = 1$, and are sorted in magnitude as $n_1(t) \geq n_2(t) \geq \dots$ without loss of generality. The eigenvalues $n_j(t)$ are named the natural occupations, and they characterize the degree of condensation and fragmentation of the condensate. Hence, when the system with one-body RDM has only a single macroscopically-contributing eigenvalue $n_1(t)$, the system is said to be condensed [53]. When the one-body RDM has k macroscopically-occupied eigenvalues, the system is referred to as k -fold fragmented [54].

2. Many-particle variances

The many-particle variance of a many-particle observable $\hat{O} = \sum_{j=1}^N \hat{o}(\mathbf{r}_j, t)$ is given as [55]

$$\begin{aligned} \frac{1}{N} \Delta_{\hat{O}}^2 &= \frac{1}{N} \left[\langle \Psi | \hat{O}^2 | \Psi \rangle - \langle \Psi | \hat{O} | \Psi \rangle^2 \right] = \\ &= \frac{1}{N} \left\{ \sum_j n_j(t) \int d\mathbf{r} \phi_j^{*(NO)}(\mathbf{r}, t) \hat{o}^2 \phi_j^{(NO)}(\mathbf{r}, t) - \left[\sum_j n_j(t) \int d\mathbf{r} \phi_j^{*(NO)}(\mathbf{r}, t) \hat{o} \phi_j^{(NO)}(\mathbf{r}, t) \right]^2 \right. \\ &\quad \left. + \sum_{jklm} \rho_{jklm}(t) \left[\int d\mathbf{r} \phi_j^{*(NO)}(\mathbf{r}, t) \hat{o} \phi_l^{(NO)}(\mathbf{r}, t) \right] \left[\int d\mathbf{r} \phi_k^{*(NO)}(\mathbf{r}, t) \hat{o} \phi_m^{(NO)}(\mathbf{r}, t) \right] \right\}. \quad (19) \end{aligned}$$

The expectation value of $\hat{O} = \sum_{j=1}^N \hat{o}(\mathbf{r}_j, t)$ depends only on the one-body operator, whereas the expectation of \hat{O}^2 is a combination of one- and two-body operators, $\hat{O}^2 = \sum_{j=1}^N \hat{o}^2(\mathbf{r}_j, t) + \sum_{j < k} 2\hat{o}(\mathbf{r}_j, t)\hat{o}(\mathbf{r}_k, t)$. $\rho_{jklm}(t)$ are the two-particle RDM, $\rho(\mathbf{r}_1, \mathbf{r}_2, \mathbf{r}'_1, \mathbf{r}'_2; t) = \sum_{jklm} \rho_{jklm}(t) \phi_j^*(\mathbf{r}, t) \phi_k^*(\mathbf{r}, t) \phi_l(\mathbf{r}, t) \phi_m(\mathbf{r}, t)$.

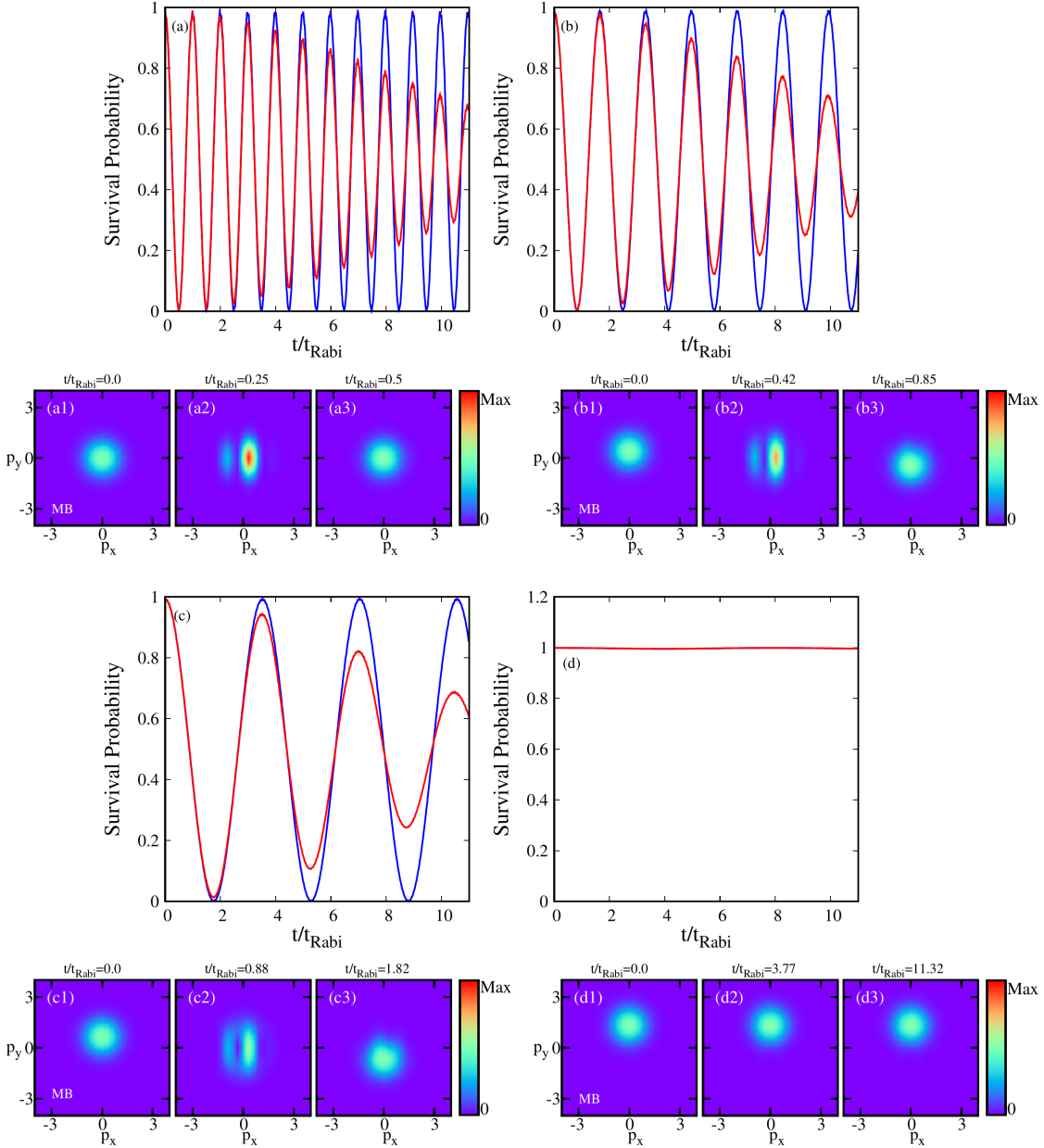


FIG. 5. Time-dependent survival probability characterizing the Josephson dynamics in position space and time snapshots of the momentum-density profile in the double well potential are shown. Panel (a) corresponds to the survival probability and panels (a₁)–(a₃) depict the momentum density for $\Omega = 0$. Panel (b) corresponds to survival probability and panels (b₁)–(b₃) depict the momentum density for $\Omega = 0.2$. Panel (c) corresponds to survival probability and panels (c₁)–(c₃) depict the momentum density for $\Omega = 0.3$. Panel (d) corresponds to survival probability and panels (d₁)–(d₃) depict the momentum density for $\Omega = 0.5$. The blue colored line depicts the mean-field dynamics and the red colored one represents the many-body dynamics. All quantities are dimensionless.

S2. DYNAMICS OF ROTATING BOSONS IN A DOUBLE-WELL POTENTIAL

In this section, we discuss in detail the impact of rotation on the bosons trapped in a double-well potential, given by Equation (5). Let us first discuss the behavior of survival probabilities that quantifies the dynamics of bosons in position space at different rotation frequencies Ω . At $\Omega = 0$, the usual Josephson tunneling of interacting bosons is observed at both the mean-field and many-body levels, Fig. 5(a). In the short-time dynamics, it is observed that both the mean-field and many-body dynamics of the survival probabilities nicely coincide with each other, indicating the presence of Rabi-like oscillations. The discrepancy between the mean-field and many-body dynamics becomes prominent in long-time dynamics. The mean-field dynamics retains constant amplitude irrespective to time increment. However, the many-body dynamics indicates a signature of quantum correlations in terms of incomplete tunneling of the bosons. The decay of the amplitude of the many-body dynamics signifies a collapse in the density oscillations. The tunneling period increases with rotation frequencies Ω , Fig 5(b)-(c). Here, the period of oscillations increases linearly with Ω . However, the mean-field and many-body dynamics retain the original amplitude of non-rotating dynamics irrespective of the increment in Ω . Finally, for the critical rotation frequency $\Omega_c = 0.5$, tunneling collapses completely; Fig. 5(d). Hence, the amplitude of the mean-field and many-body dynamics stays at 100% at all times, thus signaling the onset of self-trapping. Here, all the bosons are localized in the left well with the increase of the centrifugal barrier for strong rotation. In short, the rotation kills off the dynamics in the double-well.

To explore the effect of rotation on the momentum-space dynamics of bosons in a double-well trap, let us analyze the time snapshots of the momentum-density at different Ω . The one-body density RDM of the N-boson state $|\Psi\rangle$ in momentum space is defined as

$$\tilde{\rho}^{(1)}(\mathbf{p}, \mathbf{p}'; t) = \langle \Psi | \hat{\Psi}^\dagger(\mathbf{p}') \hat{\Psi}(\mathbf{p}) | \Psi \rangle = \sum_{k,q} \rho_{kq} \phi_k^*(\mathbf{p}', t) \phi_q(\mathbf{p}, t) \quad (20)$$

with momentum space eigenbasis $\{\phi_q(\mathbf{p}, t)\}$. Hence, the momentum-space eigenvalue representation of one-body RDM is given by

$$\frac{\tilde{\rho}^{(1)}(\mathbf{p}, \mathbf{p}'; t)}{N} = \sum_j n_j(t) \phi_j^{(NO),*}(\mathbf{p}', t) \phi_j^{(NO)}(\mathbf{p}, t). \quad (21)$$

Figs. 5(a1)-(a3) display the various time snapshots of the many-body momentum densities per particle, $\frac{1}{N} \tilde{\rho}(\mathbf{p}, t)$ calculated at three stages of the first cycle in tunneling dynamics

of the double-well trap for different Ω . In the non-rotating frame, we observe a smaller degree of displacement of the momentum-density along p_x . However, this displacement does not signify tunneling of bosons. As rotation is slowly introduced into the condensate, the momentum density is translated in $\pm p_y$ directions. However, no junction is observed in the momentum space, which is confirmed by the adjoint density profile. For significant rotation, $\Omega = 0.3$, a single-core stationary density profile is observed along the p_y direction. Since we cannot go beyond $\Omega_c = 0.5$, hence in the double-well trap, Ω_c does not induce enough rotation to observe the Josephson effect in momentum space.

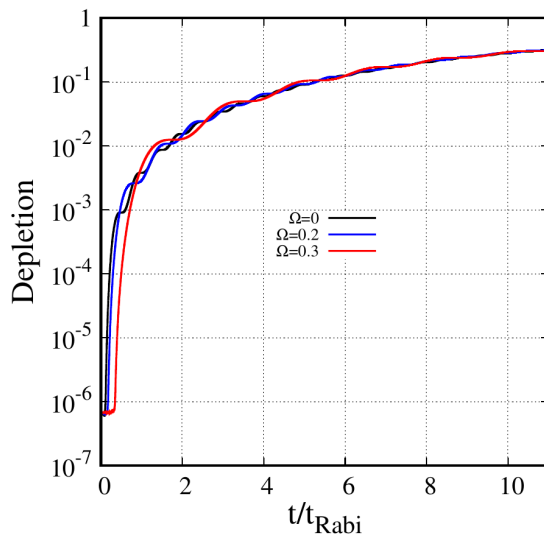


FIG. 6. Behavior of depletion as a function of time at various rotation frequencies Ω for $N = 10$ bosons with interaction strength $\Lambda = 0.04$ confined in a double-well trap. The depletions for all Ω closely follow each other. All quantities are dimensionless.

We further explore the impact of rotation on the dynamics of fragmentation of the condensate in the double-well trap. To quantify the degree of fragmentation in a condensate, the depletion per particle is an important quantity, which is defined as

$$\text{Depletion} = 1 - \frac{n_1(t)}{N}. \quad (22)$$

Here, $n_1(t)$ is the largest occupation number obtained from diagonalization of the reduced one-body reduced density matrix in Eq.(18). Basically, fragmentation defines the macroscopic occupation of more than one eigenvalue of the reduced one-particle density matrix in Eq. (18). The time development of the depletion at different rotation frequencies Ω is shown

in Fig. 6. It is observed that the depletion corresponding to $\Omega = 0$, $\Omega = 0.2$, and $\Omega = 0.3$ nicely follow each other. In a double-well trap, the rotation is found to have no discernible effect on the time evolution of depletion. The consistent amplitude of the many-body dynamics of survival probability at various Ω is complemented by this unaltered behavior of the rate of depletion with rotation.

S3. CONVERGENCE OF THE JOSEPHSON DYNAMICS UNDER ROTATION WITH RESPECT TO THE NUMBER OF TIME-ADAPTIVE ORBITALS

In this section, we report the convergence of the many-body dynamics of bosons under rotation with respect to the number of self-consistent orbitals.

A. Survival Probability

Here, we discuss the convergence of survival probabilities for two cases, namely (1) the protocol to generate Josephson junctions, shown in Figs. 7(a)-(b), and (2) the barrierless trap in Figs. 7(c)-(d) for various rotations Ω .

The survival probability in the left well of a general double-well trap quantifies the tunneling of a significant number of bosons from the right to the left well and is determined by,

$$P_L(t) = \int_{-\infty}^0 \int_{-\infty}^{+\infty} dx dy \frac{\rho(x, y; t)}{N}, \quad (23)$$

where $\rho(x, y; t)$ is the density of the bosonic cloud at a particular instant of time t , when the left well is significantly occupied by the bosons.

Looking at Fig. 7, it is observed that the dynamics of survival probabilities are fully converged with respect to the number of natural orbitals M in the rotating frame. For the convergence check of the first case, the $M = 6$ and $M = 10$ self-consistent orbitals are employed. In Fig. 7(b), for fast rotation, there is a small difference between the survival probabilities corresponding to $M = 6$ and $M = 10$ orbitals. To confirm convergence, we further simulated the survival probability for $\Omega = 0.7$ with $M = 12$ orbitals, and full convergence with $M = 12$ orbitals is observed.

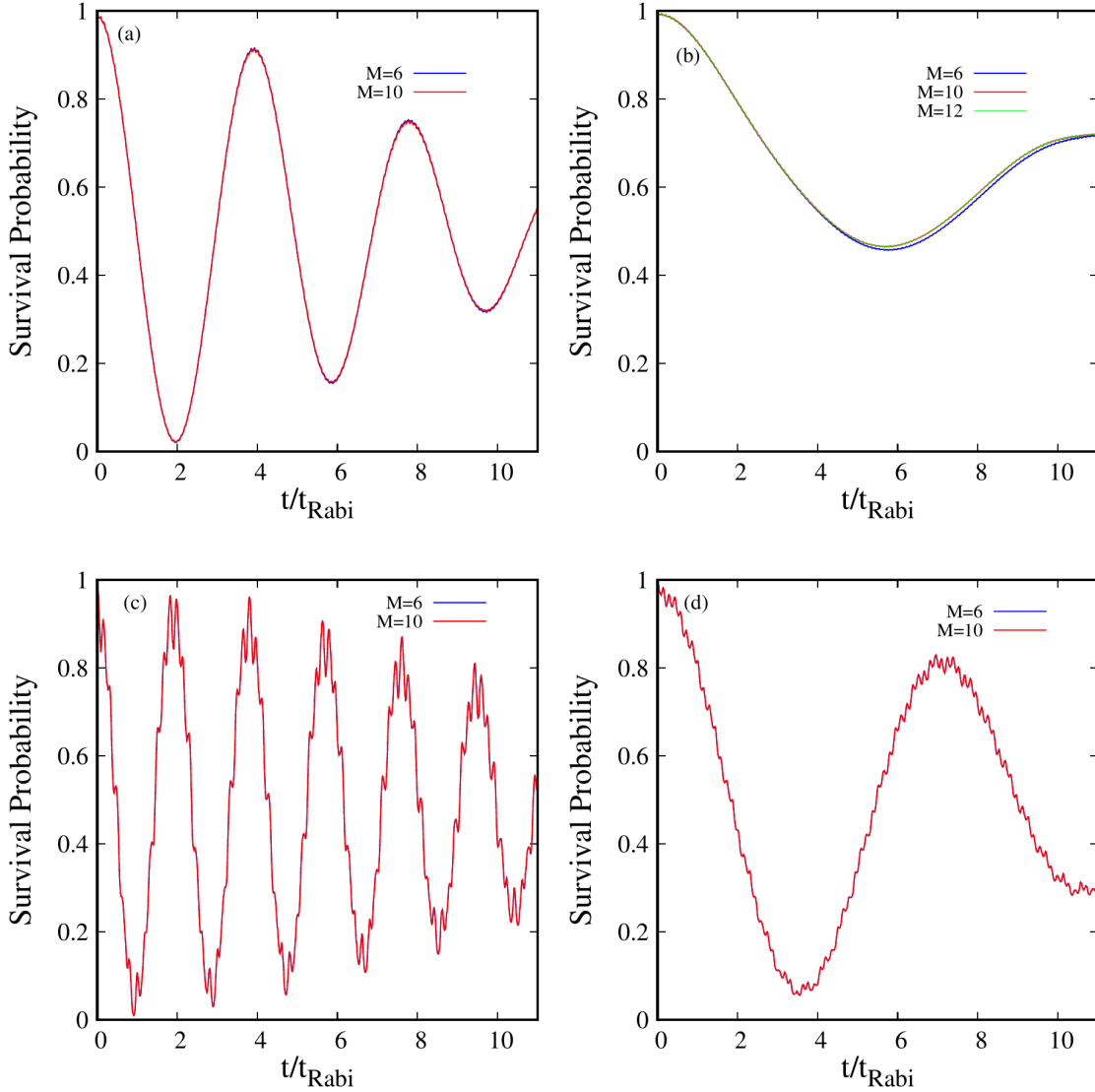


FIG. 7. Convergence of the time evolution of the survival probabilities with respect to different number of natural orbitals. The convergence check in the protocol to generate Josephson junction is shown for rotation frequencies (a) $\Omega = 0.5$ with $M = 6, 10$ orbitals and (b) $\Omega = 0.7$ for $M = 6, 10, 12$ orbitals. Similarly, (c) $\Omega = 0.45$ and (d) $\Omega = 0.5$ present the convergence of the survival probabilities in the case of the barrierless trap. All quantities are dimensionless.

B. Depletion

Fig. 8 displays the convergence of the depletion dynamics for the two cases, namely, (1) the protocol to generate the Josephson junction and (2) the barrierless trap at various rotation frequencies Ω with respect to the number of orbitals. The convergence of the

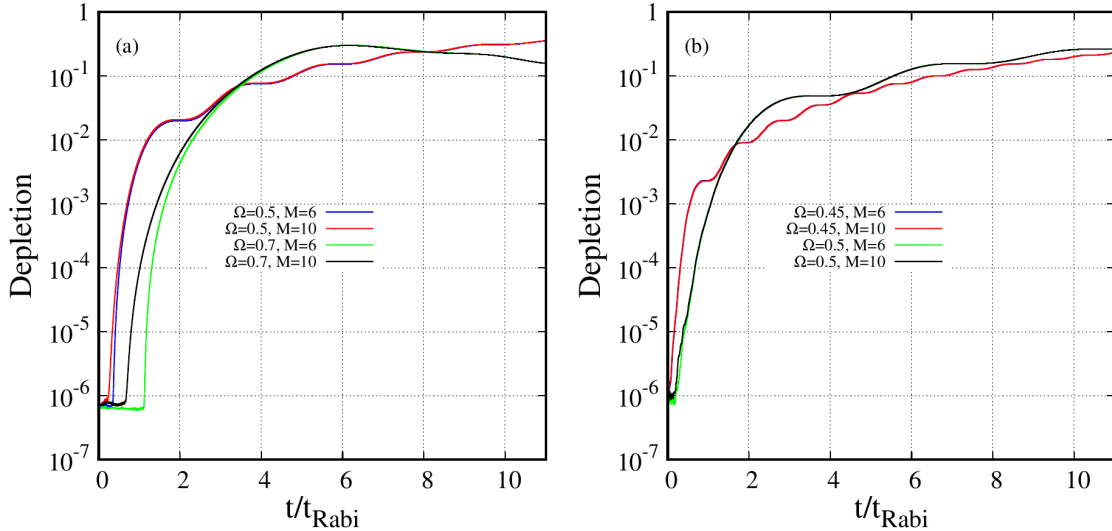


FIG. 8. Convergence of the time-dependent depletion with respect to the number of natural orbitals M , in the rotating frame for various rotation frequencies are shown. Panel (a) correspond to the protocol to generate Josephson junction and panel (b) to the barrierless trap. To check the convergence, $M = 6$ and $M = 10$ self-consistent orbitals are used. All quantities are dimensionless.

time-dependent depletion in the rotating frame is evident.

C. Many-particle variances

In this section, we report the convergence of the many-particle variances of the position and momentum operators [56, 57] for the two protocols in the rotating frame with respect to the number of orbitals M . Fig. 9 presents the convergence of the many-particle position variances $\frac{1}{N}\Delta_{\hat{X}}^2$, $\frac{1}{N}\Delta_{\hat{Y}}^2$ and the many-particle momentum variances $\frac{1}{N}\Delta_{\hat{P}_X}^2$, $\frac{1}{N}\Delta_{\hat{P}_Y}^2$ with $M = 6$ and $M = 10$ self-consistent orbitals for the two protocols, at various rotation frequencies Ω .

It is evident that the convergence with respect to the number of orbitals for the many-particle variances of the position and momentum operators for both cases is excellent.

S4. CONVERGENCE OF THE JOSEPHSON DYNAMICS IN THE ROTATING FRAME WITH RESPECT TO DIFFERENT NUMBERS OF GRID POINTS

Finally, we demonstrate the convergence of the results described in the main text with respect to the number of grid points. So far, all the results for the Josephson tunneling scenarios were computed with 64×64 grid points in the main text. To verify convergence with respect to the grid size, we recomputed the dynamics of depletion and of the many-particle position variances $\frac{1}{N}\Delta_{\hat{X}}^2$, $\frac{1}{N}\Delta_{\hat{Y}}^2$ and the momentum variances $\frac{1}{N}\Delta_{\hat{P}_X}^2$, $\frac{1}{N}\Delta_{\hat{P}_Y}^2$ for the grid points 128×128 in the case of the protocol based on double-well potential. The overlapping curves of the depletion, $\frac{1}{N}\Delta_{\hat{X}}^2$, $\frac{1}{N}\Delta_{\hat{Y}}^2$, and of $\frac{1}{N}\Delta_{\hat{P}_X}^2$, $\frac{1}{N}\Delta_{\hat{P}_Y}^2$, for increasing number of grid points signify that the results are already fully converged with grid points 64×64 .

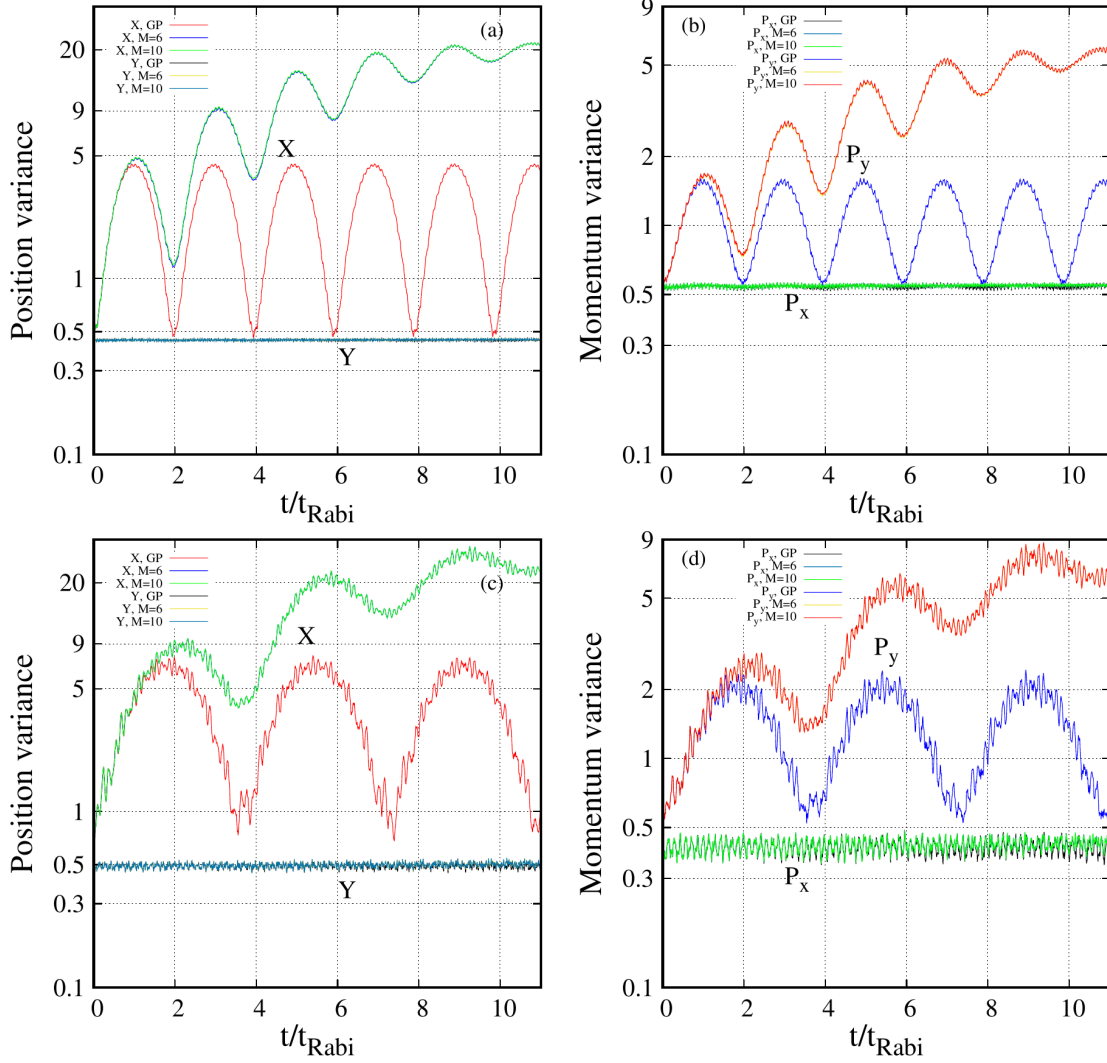


FIG. 9. Convergence of the time-dependent many-particle position and momentum variances per particle along the x and y directions, $\frac{1}{N}\Delta_X^2$, $\frac{1}{N}\Delta_Y^2$, with respect to the number of natural orbitals M in the rotating frame. Panels (a) corresponds to the many-particle position variances along the x and y directions, and (b) corresponds to the many-particle momentum variances along p_x and p_y directions, with $\Omega = 0.5$ for the double-well-based protocol. Similarly, panel (c) corresponds to the many-particle position variances along the x and y directions and (d) corresponds to the many-particle momentum variances along the p_x and p_y directions with $\Omega = 0.5$ for the barrierless trap. All quantities are dimensionless.

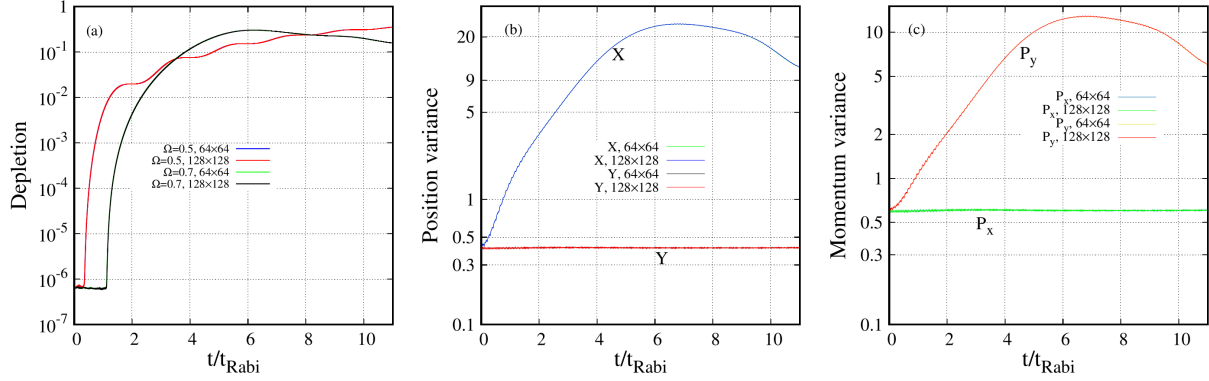


FIG. 10. Convergence of the depletion and of the many-particle position and momentum variances with respect to different numbers of grid points, different rotation frequencies Ω , are shown for the double-well-based protocol. Panels (a) corresponds to the time evolution of the depletion for various Ω , (b) represents the dynamics of the many-particle position variances along x and y directions, and (c) depicts the many-particle momentum variances along p_x and p_y directions at $\Omega = 0.7$. To check the convergence, 64×64 and 128×128 grid points are used. All quantities are dimensionless.